Spin fluid dynamics observed by magnetic fountain effect and mechanical spin pumping effect in the ferromagnetic superfluid ^{3}He A_1 phase

Y. Aoki,* A. Yamaguchi,† K. Suzuki, and H. Ishimoto
Institute for Solid State Physics, Kashiwa, Chiba 277-8581, Japan

H. Kojima
Serin Physics Laboratory, Rutgers University, Piscataway, New Jersey 08854, USA

(Received 29 May 2010; published 31 August 2010)

Systematic observations of the magnetically generated fountain pressure in the superfluid ^{3}He A_1 have been carried out in a newly built apparatus designed to reduce the effect of thermal gradients. In the same apparatus, mechanical pumping and filtering of polarized nuclear spins were realized by the pneumatic pumping action of an electrostatically actuated membrane. In both experiments, the measured induced pressure was observed to decay at all temperatures where the A_1 phase appeared in magnetic fields up to 13 T and liquid pressures between 1 and 29 bar. The inferred spin-relaxation rate tended to increase as the low-temperature phase boundary with the A_2 phase (T_{C2}) was approached. The increase in spin-relaxation rate near T_{C2} can be explained by the presence of a minority spin condensate in the A_1 phase as predicted by Monien and Tewordt and by the application of the Leggett-Takagi theory of spin relaxation in superfluid ^{3}He.

DOI: 10.1103/PhysRevB.82.054527 PACS number(s): 67.30.−n, 67.90.+z

I. INTRODUCTION

The superfluid phases of liquid ^{3}He appear below a pressure-dependent transition temperature T_C. In zero applied magnetic field two phases exist and are known as the A (having spin pairings in opposite directions but equal energy gaps: $\Delta_{\uparrow\uparrow}=\Delta_{\downarrow\downarrow}$) and the B (having all spin pairings with energy gaps, $\Delta_{\uparrow\uparrow}$, $\Delta_{\downarrow\downarrow}$ and $\Delta_{\uparrow\downarrow}$) phases. The A phase occurs only at relatively high pressures and temperatures and shares a triple point in a pressure-temperature phase diagram with the B and the normal (N) phases near 21 bar. Under applied magnetic field, the phase diagram sheds the triple point and acquires a new A_1 phase between two transition temperatures T_{C1} and T_{C2} [where $T_{C2}<T_C<T_{C1}$)] at all pressures.[1,2] The A_1 phase has been regarded as a "ferromagnetic" superfluid phase whose condensate only involves totally spin polarized pairs with the energy gap $\Delta_{\uparrow\uparrow}\neq 0$ but $\Delta_{\downarrow\downarrow}\equiv 0$.[3] Unique magnetohydrodynamics[4] of the A_1 phase leads to such effects as the spin-entropy waves,[5,6] the magnetic fountain effect (MFE),[7,8] spin-current induced electric fields[9] and the excitation of spin and mass supercurrents via the Aharonov-Casher effect.[10] The latter two have not yet been observed experimentally to our knowledge. Under an applied magnetic field and below T_{C2} $\Delta_{\downarrow\downarrow}$ begins to grow in the phase known as A_2. The magnetohydrodynamics effects listed above are absent in the A_2 phase.

Although the spin fluid dynamics of the A_1 phase have been studied over many years, there still remain outstanding questions.[11] The most important among these questions is the origin of the unexpected spin relaxation observed in MFE experiments. Understanding this spin relaxation would yield important clues in designing a spin-pumping device for boosting the spin polarization to much greater level than feasible by available static magnetic fields.[12] In this report, we describe our recent experiments on both magnetically and mechanically driven spin superflows in the superfluid ^{3}He A_1 phase. In these experiments, the underlying principle for observing the spin superfluid dynamics is the mechanical detection of the spin-density variation. Measurements were made on the A_1 phase under pressures between 1 and 29 bar and static magnetic fields up to 13 T. Improvements to the apparatus have eliminated the thermal gradients that marred an earlier experiment and precluded us from acquiring an accurate measure of the temperature dependence of the spin relaxation. From an analysis of the measured decay of the pressure change induced by applying a magnetic field gradient or by spin pumping, the spin-relaxation time (T_1) is extracted. The extracted T_1 decreases monotonically as the temperature is lowered and tends to vanish at T_{C2}. This behavior is *unexpected* for a totally ferromagnetic superfluid A_1 phase but is consistent with the A_1 phase containing a small amount of minority spin-pair condensate.[13] The presence of minority condensate is in agreement also with the theoretical predictions of Monien and Tewordt (MT).[14]

This report is organized as follows. In Sec. II, the magnetic fountain and spin-pumping effects are described in terms of simple two fluid model equations applied to our experimental apparatus. Spin relaxation is incorporated into this model phenomenologically, so as to account for the characteristic time scale over which induced spin pressures are observed to decay. In Sec. III, the details of the apparatus are described. In Sec. IV, results and analyses are presented and the paper concludes with a summary in Sec. V.

II. TWO FLUID HYDRODYNAMICS OF MAGNETIC FOUNTAIN AND MECHANOSPIN EFFECTS

Consider a small detector chamber enclosed except for an opening to the narrow channels of an attached superleak. The superleak channels connect the detector interior to a large reservoir volume. The detector chamber, superleak channels, and the reservoir volume are all filled with liquid ^{3}He. The flow impedance of the superleak is such that the normal fluid flow is severely restricted by both the large shear viscosity of

 ©2010 The American Physical Society

normal liquid ^{3}He at low temperatures and the large flow impedance of the long narrow opening in the superleak structure. One wall of the detector chamber is a stretched flexible membrane. The differential pressure between the interior of the detector chamber and the reservoir produces a membrane deflection which can be measured. In the quasistatic limit (where the superfluid acceleration is negligible), the superfluid maintains equality of chemical potential across the ends of the superleak[4]

$$\frac{\delta P}{\rho} = \frac{\gamma\hbar}{2m}\left[\delta H - \frac{\gamma}{\chi}\delta S\right], \tag{1}$$

where $\delta P \equiv P_R - P_D$, $\delta S \equiv S_R - S_D$, and $\delta H \equiv H_R - H_D$ are the differential pressure, spin density, and external magnetic field, respectively, along the superleak channels between the reservoir (R) and detector (D) ends, m is the mass of ^{3}He atom, ρ is the mass density, γ is the magnitude of the gyromagnetic ratio, and χ is the magnetic susceptibility.

If a magnetic field gradient is applied across the superleak in an ideal arrangement where the membrane deflection is negligible ($\delta S=0$), a pressure gradient is developed according to Eq. (1). This is the MFE.[4] It is also possible to apply a pressure gradient across the superleak in the absence of magnetic field gradient. In this case Eq. (1) implies that a spin-density gradient should result. We call this a mechano-spin effect (MSE).[15]

Since the volume of the reservoir is much larger than that of the detector chamber in our experiments (by at least a factor of 50), it is assumed that P_r and S_r remains effectively constant. If entropic effects are significant, the term $c\delta T$, where c is the specific heat per unit mass and T is temperature, should be added to the right side of Eq. (1). In all of our experiments, the entropic effects are negligible. Equation (1) provides the basis for the differential pressure sensor acting as a mechanical spin-density detector in the superfluid ^{3}He A_1 phase.

The average deflection Z of the differentia pressure sensor membrane (area A_m and tension σ) is related to the differential pressure δP. If an external force F_e is applied

$$8\pi\sigma Z = A_m \delta P + F_e. \tag{2}$$

If F_e is known, Z gives a direct measure of the differential pressure. Equation (2) assumes that, under deflection, the cross section of the circular detector membrane is parabolic.

The superleak consists of a stack of n channels each of width w, length L, and height $h \ll w, L$. Since it is imperfect, the differential pressure produces a small concurrent normal fluid flow (with velocity v_n) such that

$$\frac{\delta P}{\rho} = -GLv_n, \tag{3}$$

where $G=12\eta/\rho_n h^2$, ρ_n is the normal component density, and η is the normal component shear viscosity.

The total mass flow in the superleak is related to the membrane deflection by the conservation of mass

$$\rho A_m \dot{Z} = (\rho_s v_s + \rho_n v_n)A, \tag{4}$$

where ρ_s is the superfluid component density, v_s the superfluid component velocity and $A=nwh$ is the total cross-sectional area of the superleak.

Finally, changes in δS can be generated by a flow of the spin-polarized superfluid component flow in and out of the detector chamber. If the superflow were the only source of change, δS and δP should become constant when the superflow ceases since the balance condition expressed by Eq. (1) is established under a constant applied δH. In our experiments, δP is always observed to decay to zero. To incorporate a phenomenological description of this relaxation, the effects of spin-density relaxation and spin diffusion are added to the net change in δS. The net rate of change in spin-density difference is written as

$$\delta\dot{S} = \frac{\rho_s \hbar A}{2mV} v_s + \left(\frac{\chi}{\gamma}\delta H - \delta S\right)\frac{1}{T_1}, \tag{5}$$

where V is the volume of the detector chamber and T_1 is the spin-relaxation time. The spin current $S_n v_n = (\chi\delta H/\gamma)v_n$ contributed by the normal fluid flow is negligibly small. Equation (5) ensures that the membrane dynamics are coupled to those of the spin-density and the normal fluid flow.

Equations (1)–(5) are a closed set of equations governing the time (t)-dependent response of the detector membrane to externally applied δH and F_e. The response $Z(t)$ to a step change in δH (keeping $F_e=0$) is a simple exponential function with a time constant τ given by

$$\frac{1}{\tau} = \left(\frac{1}{\tau_n} + \frac{\alpha}{T_1}\right)\left(\frac{1}{\rho_n/\rho + \alpha}\right), \tag{6}$$

where

$$\tau_n = \frac{A_m^2 \rho L G}{8\pi\sigma A} \tag{7}$$

is the normal fluid flow relaxation time and

$$\alpha = \frac{32\pi\sigma\chi m^2 V}{\hbar^2\gamma^2\rho\rho_n A_m^2} \tag{8}$$

is the mechanical to magnetic energy density ratio. Since ρ_s is quite small in the A_1 phase, ρ_n may be approximated by ρ. If a step force F_e is applied to the membrane instead of step magnetic field gradient, the MSE is observed. The response is again a simple exponential with the *same* time constant as given by Eq. (6). From the measured relaxation time τ, the spin-relaxation time T_1 is extracted using Eq. (6).

The ratio α can be evaluated from the known cell dimensions and liquid parameters.[1] It can also be determined empirically as follows. Let us suppose that $\delta H=0$ and that F_e has been applied for a sufficiently long time for equilibrium to be established between the detector chamber and the reservoir; hence $\delta P=0$ (and $\delta S=0$). When F_e is removed at $t=0$, δP begins to develop and the superfluid accelerates out of the detector chamber. The superflow out of the chamber is a totally spin-polarized flow. Let Z_0 be the initial membrane displacement before F_e is removed, and let Z_1 be the displacement at the time $t=t_1$ when the acceleration ceases and

a quasistatic equilibrium is established. During a short time period ($\ll\tau$), if the normal flow and spin relaxation are both negligibly small, $\delta S=(\rho\hbar A_m/2\ \mathrm{mV})(Z_1-Z_0)$ and $\delta P=-(\rho\hbar\gamma^2/2m\chi)\delta S$ at $t=t_1$. Using Eq. (2) to relate δP to Z, it can be shown

$$Z_1=\frac{1}{1+\alpha}Z_0. \tag{9}$$

This relation is used to determine α from measurements of Z_0 and Z_1.

In the normal and A_2 phases, the broken relative spin-gauge symmetry on which Eq. (1) is based is no longer applicable and MFE is not expected to be present[4] in accordance with experiments.[16] The appearance of the MFE and/or the MSE serves as clear markers for the presence of the A_1 phase.

III. EXPERIMENTS

A. Motivation for improving the previous apparatus

As evident from the previous section, the relaxation time τ plays a key role to understanding the magnetically driven superflow and magnetic fountain pressure effects in the A_1 phase. In our recent study of MFE, the measured values of τ decreased toward zero with a peculiar, possibly extrinsic, kink (see Fig. 2 of Ref. 13) in its temperature dependence as T_{C2} was approached. Since establishing the intrinsic temperature dependence of τ is very important and it may affect our conclusion on the existence of a minority spin condensate, it is imperative to investigate the kink in the temperature dependence of τ.

To study the possibility of a thermal gradient across the superleak as the source of the observed kink in τ, a new apparatus was constructed in an essentially identical manner to the previous one[13] using the epoxy Stycast 1266 as the construction material (see below). In addition two vibrating wire viscometer thermometers were installed; one in the detector chamber and the other in the reservoir.[17] The kink (at $r\approx 0.35$) in the temperature dependence of τ was indeed reproduced in the new apparatus as shown in Fig. 1 where $r\equiv(T-T_{C2}^D)/(T_{C1}^D-T_{C2}^D)$ is a normalized reduced temperature. Figure 1 also shows the simultaneously measured oscillation amplitude of the vibrating wire placed in the reservoir. The phase transition temperatures, T_{C2}^D and T_{C1}^D, in the detector region, were defined by the appearance and disappearance of the MFE signal, respectively, as the sample warmed. The presence of the A_1 phase (between T_{C2}^R and T_{C1}^R) in the reservoir can be clearly identified by the kinks in the viscometer oscillation amplitude. Note that the MFE appears at an earlier time than T_{C2}^R. This shows that the liquid within the detector chamber is in fact warmer than in the reservoir. Furthermore, the kink in the observed temperature dependence of τ coincides with T_{C2}^R. Evidently, the kink occurs when the liquid in the reservoir chamber makes a transition into the A_1 phase. The temperature gradient likely occurs within the superleak channels. The interface between the A_1 phase and the A_2 phase then advances along the superleak from the detector volume side to the reservoir volume as the experiment

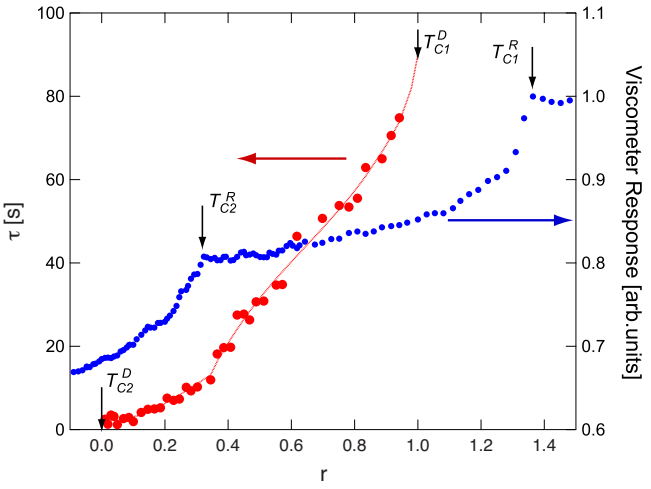

FIG. 1. (Color online) Relaxation time τ vs normalized reduced temperature r (large red circles; see text) and viscometer oscillation amplitude (small blue circles). These data were taken during a slow warming period. The coincidence of the kink in τ and T_{C2}^R at $r\approx 0.35$ is clearly evident. $P=21$ bar, $\mu_0 H=8$ T (μ_0 is the permeability of free space).

shown in Fig. 1 progresses. This A_1-A_2 interface might be an interesting object for study in its own right.[18,19] However, it is now clear that the temperature gradient needs to be reduced for proper measurement of the temperature dependence of τ. The next section describes how this was accomplished.

B. Improved apparatus

The Stycast 1266 epoxy used for fabricating the parts of apparatus was suspected as the source of long term heat release and thermal gradients.[20] With this in mind, almost all components of the new apparatus as shown in Fig. 2 were reconstructed using the machinable ceramic Macor as the fabrication material. Stycast 1266 and 2850 were used sparingly only for gluing some of the parts together. These efforts apparently paid off since the temperature gradient effects observed using the previous apparatus are now essentially nonexistent as described below.

The liquid ^{3}He contained in volume (a) in Fig. 2 is linked via a liquid column in an 8 mm innerdiameter interconnecting tower (b) to a sintered heat exchanger in good thermal contact with a powerful copper nuclear demagnetization cooling stage. All of the liquid ^{3}He associated with the experiment is exposed to an external static magnetic field applied along the vertical axis of the apparatus with uniformity better than 99% over the entire liquid volume. The temperature is measured using a calibrated ^{3}He melting curve thermometer located in a low magnetic field region and in good thermal contact with the liquid.

The detector chamber body (c) is first assembled by gluing in the differential pressure sensor membrane (d) while leaving the superleak port open. Before the superleak (e) is inserted into the port, the chamber body is leak tested at 77 K to verify that there is no undesirable ancillary opening between the interior of the chamber and the outside. The super-

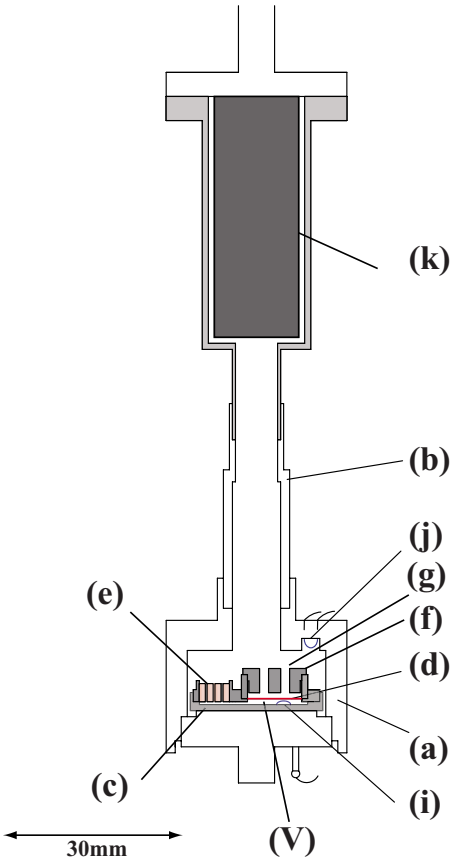

FIG. 2. (Color online) Schematic of new apparatus. The detector chamber and the ^{3}He container were fabricated from a machinable Macor ceramic. (a) Liquid ^{3}He container, (b) interconnecting tower leading to the nuclear demagnetization stage, (c) detector chamber body, (d) movable membrane, (e) superleak, (f) stationary electrode holder, (g) vent holes, (i) inner vibrating wire, (j) outer vibrating wire, (k) heat exchanger, and (v) detector chamber volume. The superleak, the distance between the movable membrane and the stationary electrode holder, and the detector chamber volume are shown enlarged for clarity.

leak is fabricated from a mold by first sandwiching $3(=n)$ of 18 μm$(=h)$ thick sheets of aluminum foil between thin Macor plates (affixed to the mold) of 3 mm in width and 3 mm$(=L)$ in length. The aluminum is then etched away, leaving a total open cross sectional area (A) of 1.6×10^{-3} cm^2. The flow impedance of the superleak was measured separately at room temperature by a gas flow test. The differential pressure sensor membrane is a 6 μm thick circular Mylar sheet coated with aluminum film on one side. Deflections of the membrane in response to the differential pressure between inside the detector chamber and the reservoir are detected by measuring the capacitance between the aluminum film electrode and a stationary electrode (f). Vent holes (g) with low flow impedance bored into the stationary electrode holder equalize the pressure just above the membrane to that in the reservoir. The active area of the Mylar membrane is 0.567 cm$^2(=A_m)$. The diameter of the stationary electrode is 8.5 mm. The measured ambient capacitance (C_0) of the differential pressure sensor at 20 mK is 17.2×10^{-12} F. The ambient average separation (d_0) between the membrane and the stationary electrode is thus estimated to be 29 μm. The displacement Z of the membrane is simply related to the measured change in capacitance δC by $Z = (\delta C / C_0) d_0$. The estimated volume (V) of the detector chamber is 0.13 cm^3. The tension (σ) of the membrane is determined to be 2.1×10^5 dyne/cm by measuring the changes in capacitance in response to applied voltages between the electrodes in liquid ^{3}He at $\sim$4 mK.

Magnetic field gradients required for observing the MFE are produced by driving currents into a set of coils designed to produce a field that varies linearly along the axis over the superleak region. The magnetic field gradient produced by the coils was measured using a Hall probe to be 26 G/Acm. The gradient coils were wound from a superconducting wire whose critical field was about 8 T. The critical field limited the highest static field at which the MFE could be studied. The MSE, on the other hand, is not limited in this way and could be studied up the highest static field of 13 T.

C. Electrostatic drive

A pressure gradient for observing the MSE is produced by applying an external voltage V_e between the two electrodes of the differential pressure sensor. The applied voltage exerts a force, $F_e = C_0 V_e^2 / 2\varepsilon A_m$ on the membrane, where ε is the permittivity of liquid ^{3}He. The deflection that is generated can be measured by monitoring the change in capacitance. The driven motion of the membrane acts as a mechanical spin pump which moves the spin-polarized superfluid component of the A_1 phase into or out of the chamber through the superleak. Although induced changes in spin polarization are small in this apparatus, the changes are sufficiently large to be used for measuring relaxation processes. As stated earlier, the MSE has an advantage over the MFE in that there is no issue with the critical current in the gradient field coils under high static magnetic fields. In a separate MSE device specifically designed to boost spin polarization, changes in polarization greater than those observed here by four orders of magnitude have been achieved.[12]

D. Normal liquid ^{3}He flow through the superleak channels

Prior to carrying out the MFE and MSE measurements, the characteristics of the superleak and the motion of the differential pressure sensor membrane are verified by observing the viscous flow of normal liquid ^{3}He through the superleak channels when subjected to a pressure difference. Equilibrium in the membrane deflection is first established for a given applied voltage V_e and liquid temperature. Subsequently, V_e is removed and δC (and hence Z) is monitored as a function of time. Apart from a small initial deviation (discussed in Sec. III F), the decay of Z is accurately exponential (see Fig. 6) with a time constant τ_n.

Measured values of τ_n at several liquid pressures are plotted against T^{-2} in Fig. 3. In the hydrodynamic regime at relatively high temperatures, τ_n is expected to be proportional to η, which varies $\propto T^{-2}$, in agreement with the data at 21 bar shown in Fig. 3. At low temperatures, where the mean-free-path length approaches the superleak channel height h, the hydrodynamic flow is modified by slip effects at

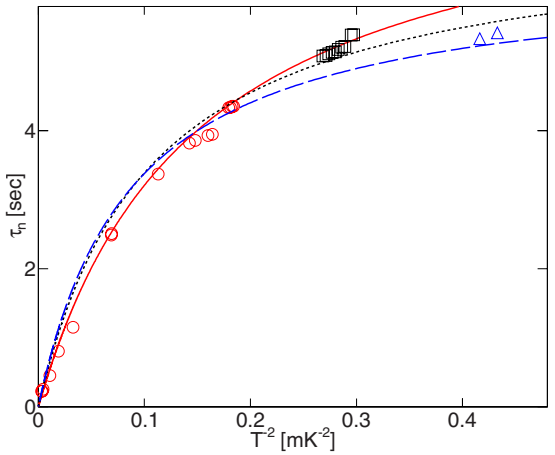

FIG. 3. (Color online) Normal liquid ^{3}He flow relaxation time τ_n vs T^{-2}. Liquid pressures are 5 (triangles, dashed line), 10 (squares, dotted line) and 21 (circles, solid line) bar. The curves represent fits (see text) to a simple theory that takes into account the slip effect at the boundary (see text).

the boundaries. The curves drawn in Fig. 3 show the expected behavior of τ_n from the "simple" slip effect theory[21] applied to rectangular channels. The inputs to the theory are the measured tension, the tabulated shear viscosity,[1] various cell dimensions as fabricated and a value for the channel height h adjusted to 17.7 μm. This adjusted value is very close to the thickness of the aluminum foil used in the construction (see above) of the superleak channels.

E. Magnetic fountain effect

After verifying the superleak characteristics, a static magnetic field is applied for measurements in the A_1 phase. A measurement run is typically started by cooling below T_{C2} into the A_2 phase. During the subsequent slow warming of the sample caused by the residual heat leak, a series of measurements of the MFE is acquired until the liquid enters the normal phase above T_{C1}. Examples of data from a typical run are displayed in Fig. 4, where the membrane displacement Z derived from δC are shown. Here, the field gradient across the superleak is increased at $t=0$ from −10.4 to +10.4 G/cm during a time interval (~0.2 s) that is short compared to the relaxation time τ. The field gradient is kept constant for a sufficient length of time for steady state to be reached. The field gradient is then decreased back to −10.4 G/cm over the same time interval as the initial increase. The same sequence of changes in field gradient is repeated throughout the run. As expected, no response is observed in the A_2 (2.07 mK) and N (2.50 mK) phases where the MFE is absent. Within the A_1 phase, the influence of the MFE is clearly seen in the response of the membrane to the superfluid motion induced by the changes in the applied field gradient. Characteristically, Z reaches a peak (Z_{max}) just after the change in field gradient and then decays exponentially with time constant τ (see Fig. 8).

The critical measure of success in reducing temperature gradients in the new apparatus is to observe the coincidence of the appearance and disappearance of the MFE signal with

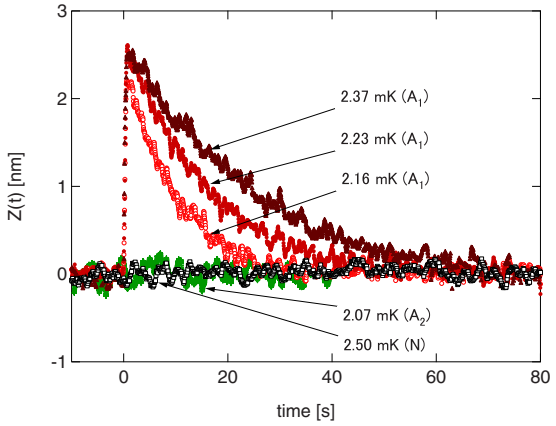

FIG. 4. (Color online) Typical membrane displacement responses during MFE experiments in the A_2, A_1, and N phases ($P=21$ bar, $\mu_0 H=8$ T). The field gradient is linearly ramped up from −10.4 to +10.4 G/cm between $t=0$ and 0.2 s.

the indications of T_{C2} and T_{C1} given to the vibrating wire viscometer in the reservoir. Figure 5 shows both the normalized viscometer response amplitude and the peak membrane displacement amplitude of Z for the same data as shown in Fig. 4. The abrupt increase and decrease in the response amplitude at T_{C2} and T_{C1} coincide within ~5 μK to the temperatures at which the kinks in viscosity occur. Similar coincidences are observed at all other applied static fields. It is clear that thermal gradients in the improved apparatus are much reduced from those in the previous apparatus (cf. Fig. 1) and that it can be said: $T_{C1}^D = T_{C1}^R \equiv T_{C1}$ and $T_{C2}^D = T_{C2}^R \equiv T_{C2}$. Care, however, still had to be exercised in limiting the excitation level in the capacitance bridge circuit.

It follows from Eqs. (1)–(5) that

$$\delta\dot{H} = aZ + b\dot{Z}, \tag{10}$$

where

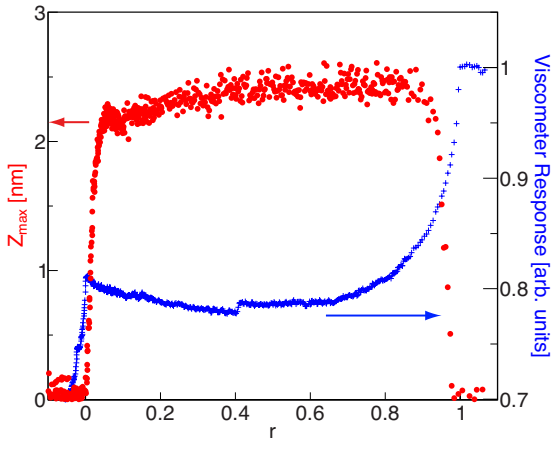

FIG. 5. (Color online) Peak amplitudes of the membrane displacement and vibrating wire viscometer responses measured during the same run as shown in Fig. 4. Coincidence of the phase boundary temperatures T_{C2} and T_{C1} for the A_1 phase as indicated by the viscometer amplitude and the MFE signal is clearly demonstrated.

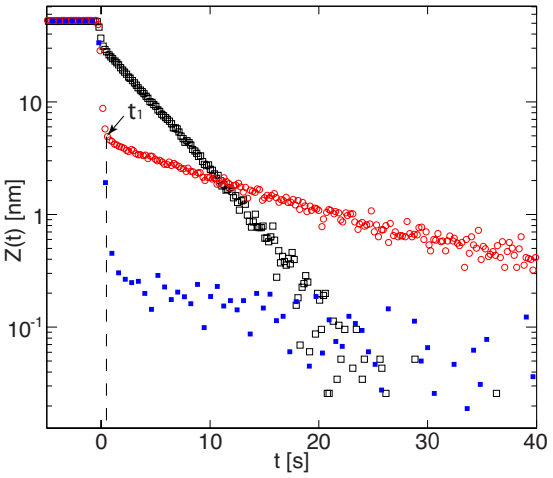

FIG. 6. (Color online) Examples of membrane displacement response after removing an applied voltage. A typical time sequence is as follows: $V_e=30$ V during $-30\ \mathrm{s}<t<0$ s, 0 V during $0\leq t<100$ s. Open black squares: normal liquid at $T=2.7$ mK, closed blue squares: A_2 phase and open red circles: A_1 phase, all at $P=21$ bar. For $t\geq t_1$, the A_1 phase response becomes quasistatic (see text).

$$a=\frac{\hbar\gamma A\rho_n 8\pi\sigma}{2m\chi VG\rho A_m L}+\frac{16m\pi\sigma}{\rho\hbar\gamma A_m \mathrm{T}_1}, \tag{11}$$

and

$$b=\frac{\hbar\gamma\rho A_m}{2m\chi V}+\frac{16m\pi\sigma}{\rho\hbar\gamma A_m} \tag{12}$$

are constants. To mimic our experiment, let $\delta H=ct$ when $0<t<t_0$ and $\delta H=ct_0$ when $t>t_0$, where c and t_0 are constants. If $t_0\ll(b/a)=\tau$, it can be shown that $Z(t=t_0)=(c/b)t_0$. Thus the peak membrane amplitude is expected to be independent of temperature and applied field if t_0 is held constant. Putting in the cell parameters to evaluate b and c, and setting $t_0=0.2$ s gives $Z(t=t_0)=2.7$ nm. Figure 5 shows that the peak displacement is indeed comparable to this estimate. As expected, the peak displacement is independent of temperature except near T_{C1}, where critical velocity effects are likely present, and near T_{C2}, where τ becomes comparable to t_0.

F. Mechanospin effect

Let us now turn to the membrane response during MSE experiments carried out *in the absence of applied magnetic field gradients*. Initially, V_e is applied for a sufficient time interval (30 s) for the membrane to come to equilibrium. $Z(t=0)$ is set by the membrane tension, $|F_e|$, and the conditions, $\delta P=0$ and $\delta S=0$. V_e is then rapidly (within 0.2 s) reduced to zero at $t\equiv 0$. This sequence is repeated (usually 10 times) so that the signal can be averaged. Typical responses to this electrostatically actuated superflow, or spin pumping, are shown in Fig. 6 for the N, A_1 and A_2 phases. In the N phase, the response is determined by the normal fluid flow, and Z decays exponentially except for an initial transient. This small initial nonexponential decrease in the membrane shape is present at all temperatures and is likely caused by some rearrangement in the membrane shape when the pressure source changes from being electrostatic to hydrostatic. The temperature dependence of the relaxation time τ_n in the N phase is shown in Fig. 3 and has already been discussed. In the A_2 phase, Z decays very rapidly to the noise floor. The rapid decay is likely limited by some critical flow effect within the superleak. Critical flow effects in superfluid ^{3}He are complicated[22] and were not studied here in detail.

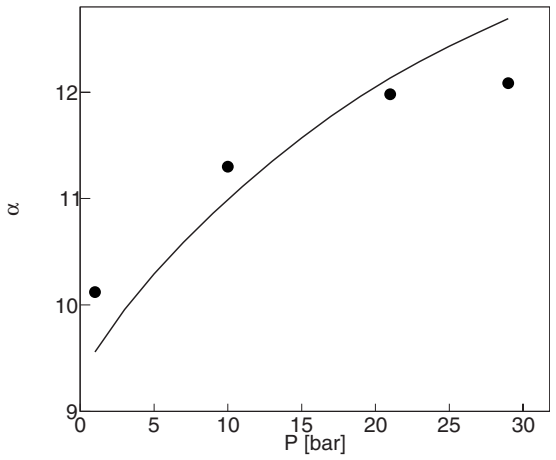

FIG. 7. Empirical determination of the magnetic to mechanical energy ratio α. The line is the expected pressure dependence from Eq. (8) multiplied by 3.3.

The time response of the membrane displacement $Z(t)$ in the A_1 phase shown in Fig. 6 is clearly distinct from those in the N and A_2 phases. There is an initial ($t<t_1$) rapid decrease in Z similar to that observed in the A_2 phase but $\dot{Z}$ abruptly changes at a specific time which we label t_1 defined above. When $t\geqq t_1$, the chemical potential is equalized across the superleak leading to a quasistatic response. $Z(t)$ at $t>t_1$ is well described by exponential decay from which τ (see Fig. 8) is extracted.

Substituting the geometric parameters of the detector, the measured membrane tension, and the liquid parameters at $P=21$ bar into Eq. (8) gives the magnetic to mechanical energy ratio $\alpha=3.68$ dyn $\mathrm{G}^2\ \mathrm{s}^4/\mathrm{g}^2$. The empirical value of α determined from $Z(0)$ and $Z(t_1)$ [see Eq. (9)] is larger than this by a factor of 3.3. The difference might arise from the assumption of a parabolic membrane shape under both hydrostatically and electrostatically applied pressures. However, the measured pressure dependence is in fair agreement with the expected pressure dependence ($\propto\chi/\rho^2$) as shown in Fig. 7. At a given pressure, α is independent of temperature, as expected, within $\pm 5\%$.

It is interesting to compare $Z(t_1)$ with the peak displacement amplitude during the MFE experiment shown in Fig. 4. $Z(t_1)$ is observed to be independent of temperature as expected. The magnitude of $Z(t_1)$ is equivalent to a change in magnetic field gradient of ~ 28 G/cm during similar experiments to those shown in Fig. 4. The change in spin density δS that would be equivalent to the pressure difference $\delta P(t=t_1)$ (cf. Fig. 6) using Eq. (1) is only 0.02% of the spin-density polarization ($=\chi H/\gamma$) produced by the applied field of $\mu_0 H=8$ T. The change in spin density δS induced by spin

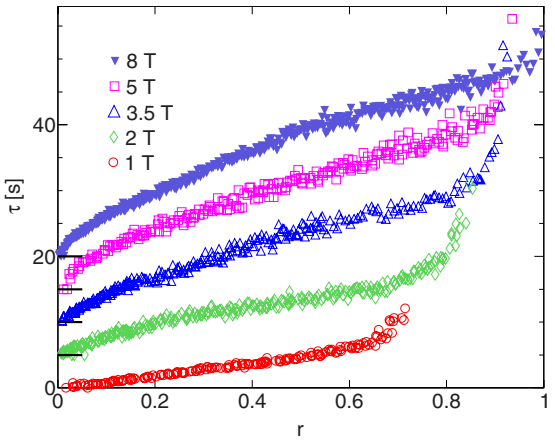

FIG. 8. (Color online) Values of τ extracted from MFE measurements vs normalized reduced temperature at $P=21$ bar and applied magnetic fields of 1 (circles), 2 (diamonds), 3.5 (upward triangles), 5 (squares) and 8 (downward triangles) T. Smooth variations in τ at all temperatures and fields are evident. For clarity, the data at 2 T and higher fields are shifted upwards by 5 s, 10 s, 15 s, and 20 s, respectively.

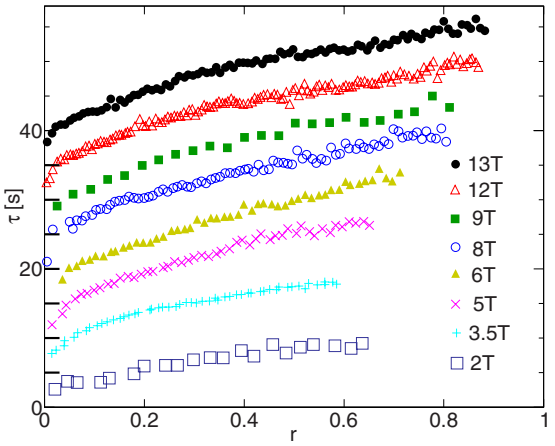

FIG. 9. (Color online) Values of τ extracted from MSE measurements vs normalized reduced temperature at $P=21$ bar and applied magnetic fields of 2 (squares), 3.5 (pluses), 5 (crosses), 6 (closed triangles), 8 (circles), 9 (closed squares), 12 (open triangles) and 13 (dots) T. For clarity, τ at 3.5 T and higher fields are shifted up by 5 s relative to the preceding data set.

pumping here is very small owing in part to the relatively large detector volume. The cooling expected from entropy dilution, $\sim T_{C1}A_m Z(t_1)/V$, is only several nanokelvin and is negligible.

IV. SPIN RELAXATION

A. Measurements

A striking feature of the MFE data shown in Fig. 4 is the exponential decay of the induced magnetic fountain pressure. Equation (1) does not imply that this decay in δP should occur. A phenomenological description of this decay was introduced above in terms of spin relaxation characterized by T_1 [cf. Eq. (6)]. The improvements made to the present apparatus (elimination of thermal gradients) enables to measure more accurately the temperature dependence of the relaxation time.

It is known that the ^{3}He spin-relaxation rate in the millikelvin temperature range is often influenced by magnetic interactions at wall boundaries.[23,24] It was found in our previous MFE experiments[8] that coating all surfaces in contact with the sample ^{3}He in the apparatus with five monolayers of ^{4}He has no significant effect on the measured relaxation time. Though such ^{4}He surface coating experiments were not carried out during the present work, we expect that they would be equally ineffective insofar as spin relaxation is concerned.

Systematic measurements characterizing the MFE similar to those shown in Fig. 4 were made as functions of applied static magnetic field and liquid pressure. Extracted decay times τ from the measurement are shown in Fig. 8, where the temperature is expressed as a normalized reduced temperature r for convenience in comparing data acquired under different applied static fields. Note the shifted ordinate scales for different applied fields. The kink in the temperature dependence of τ observed previously near $r\sim 0.4$ (see Fig. 1) is now absent. It is concluded that the kink was an artifact resulting from the inadvertent presence of temperature gradients across the superleak. Under all applied fields τ decreases monotonically toward zero as T_{C2} is approached. The previously observed tendency of τ to vanish as T decreases toward T_{C2} is confirmed in the present apparatus. Thus, the observation on which the conclusion for the presence of minority spin condensate was based, still remains valid. On the reduced normalized temperature scale, τ tends to increase more rapidly at lower fields as T_{C1} is approached. The overall dependence of τ with r varies weakly on the applied static field.

Figure 9 shows τ as measured using by the pneumatically driven MSE method is shown under magnetic fields up to 13 T and a liquid pressure of 21 bar. It can be seen that the dependence of τ on r changes somewhat at low magnetic field but becomes independent of field when $\mu_0 H \geq 5$ T. The manner in which τ increases near T_{C2} is slightly different here than in Fig. 8.

It is expected from the simple two fluid model (see above) that the time constant extracted from the MSE (cf. Fig. 9) is identical to that extracted from the MFE (cf. Fig. 8). Many of the features of τ exhibited by data associated with these two methods are similar but not identical in detail. To examine the apparent difference in the temperature dependence of τ, "simultaneous" measurements of τ were acquired using both the MFE and the MSE methods during a single run as shown in Fig. 10. The two methods were alternately applied as the temperature increased slowly. As expected, the onset of MSE and MFE occurs at the same temperature. The MSE method gives a steeper temperature dependence for τ near T_{C2} and a more gradual one near T_{C1}. These differences are not likely to be caused by temperature effects since the measurements are made alternately. With the MFE method, the applied field gradients extend over the A_1 phase in the reservoir region. Spin-relaxation effects in the reservoir, which are assumed to be negligible in our simple two fluid model, *might* bring

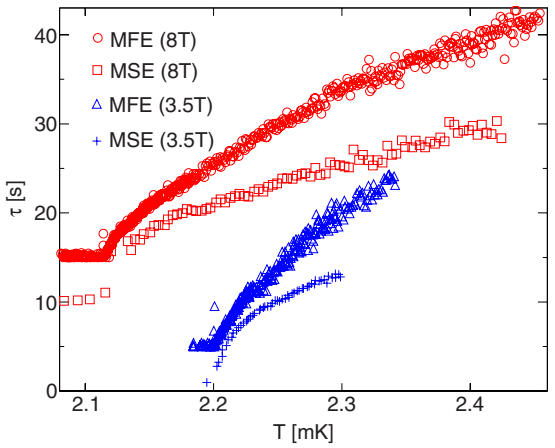

FIG. 10. (Color online) Values of τ measured simultaneously using the MFE and MSE at 8 and 3.5 T at 21 bar and acquired during the same run. Simultaneous measurements acquired at 2 and 5 T yield similar results. For clarity, the data for 3.5 T (MFE), 8 T (MSE) and 8 T (MFE) are shifted up by 5 s each.

about the difference. In the case of the MSE method, the induced spin-density gradients should be confined to the region in close proximity to the detector chamber itself.

The dependence of τ on static magnetic field at $r=0.5$ is shown in Fig. 11. Up to about 4 T, both the MFE and MSE methods exhibit the same field dependence. While the values of τ measured using the MFE method continues to increase up to 8 T, those measured using the MSE method saturate in the range $\mu_0 H \gtrsim 6$ T. Clearly, more work is needed in the high-field range. Understanding of the entire field dependence of τ is important to boosting the spin polarization achievable using spin pumping techniques.[12]

Measurements of relaxation time were also conducted using both the MFE and MSE methods at several pressures. The results are shown in Fig. 12 for an applied field of 8 T. Both methods yield a similar weak pressure dependence of τ. The inset in Fig. 11 shows the dependence for τ to pressure at $r=0.5$. At pressures above about 15 bar, τ becomes independent of pressure.

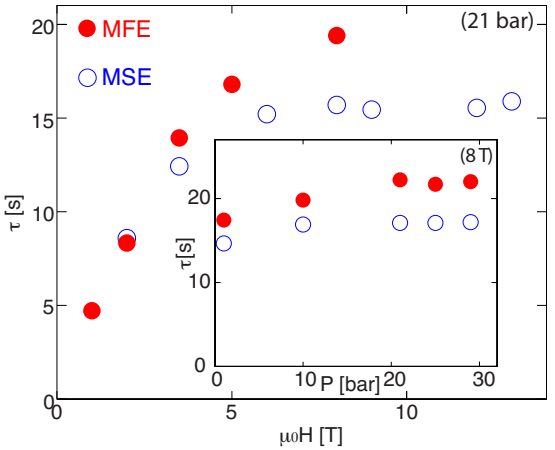

FIG. 11. (Color online) Dependence of τ on applied magnetic field at $r=0.5$ and $P=21$ bar from both the MFE and MSE measurements. Inset shows pressure dependence of τ ($r=0.5$, $\mu_0 H=8$ T).

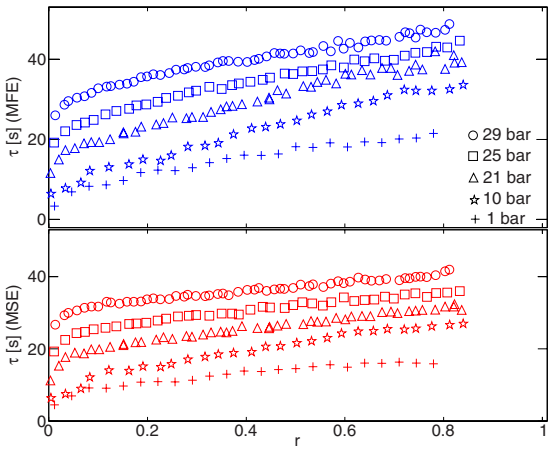

FIG. 12. (Color online) Pressure dependence of τ as inferred from both the MFE (upper panel) and MSE (lower panel) at 8 T. For clarity, the data at 10 bar and higher are each shifted upwards by 5 s relative to the previous data set.

B. Analysis

According to Eq. (6), the measured relaxation time τ depends on both the normal fluid relaxation time τ_n and the spin-relaxation time T_1. The quantity of more interest is T_1. Since τ_n remains finite at all temperatures, the observed tendency of τ to vanish at T_{C2} implies that T_1 also tends to vanish there. This surprising finding was interpreted previously[13] as a consequence of the presence of a minority spin condensate in the A_1 phase. The data acquired using the improved apparatus are carefully analyzed and their interpretation in terms of a model involving a minority spin condensate is reexamined.

To extract T_1 from the measured values of τ, the shear viscosity entering the normal relaxation time τ_n is estimated as follows. The temperature dependence of the shear viscosity $\eta(T)$ of the A_1 has been measured in high magnetic fields only at the melting pressure[25] where the ratio $\eta(T)/\eta(T_{C1})$ within the A_1 phase is a universal function of T/T_{C1} independent of magnetic field. For the analysis of our data, it is assumed that the same universal function gives good approximations for the temperature dependence of the hydrodynamic shear viscosity at lower pressures. The normal fluid shear viscosity at T_{C1} is evaluated using a tabulation of normal fluid properties.[1] The hydrodynamic shear viscosity is further corrected to account for slip effects[21] (see discussion of τ_n above) present in the superleak channels. The slip corrections are considerable at low temperatures and pressures where the mean-free path becomes large. However, it should be noted that the relatively large value of α (cf. Fig. 7) reduces the influence of τ_n on the value of T_1 from the τ data.

Figure 13 summarizes the spin-relaxation rate T_1^{-1} extracted in the manner described above from the simultaneous measurements of τ by MFE and MSE. As it was already implicitly evident from τ (shown in Fig. 10), the dependence of T_1 on r derived from the MFE and MSE methods qualitatively track one another except for two slight differences: near T_{C2} values of T_1 extracted from the MSE data are longer than those from the MFE, and near T_{C1} those from the MFE

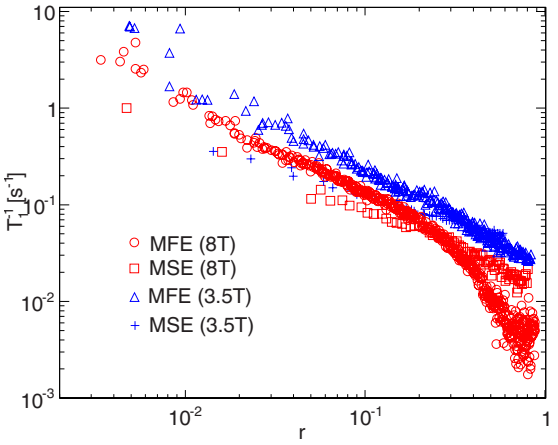

FIG. 13. (Color online) Extracted relaxation rate T_1^{-1} vs reduced temperature r. The simultaneous measurements of τ at $P=21$ bar shown in Fig. 10 are used in conjunction with Eq. (6) to extract T_1^{-1}. Symbols are the same as those used in Fig. 10.

data show stronger temperature dependence than those from the MSE data. It is clear from Fig. 13 that T_1^{-1} continues to increase as T_{C2} is approached. The maximum relaxation rate that can be measured is limited to about 10 s^{-1} by the time constant of the lock-in amplifier used for capacitance detection. No transport properties such as viscosity or spin diffusion in the A_1 phase are known to vanish or diverge at T_{C2} with the possible exception of a preliminary report by Awobode and Leggett.[26] It is concluded that the large increase in T_1^{-1} near T_{C2} originates in an intrinsic spin-relaxation process occurring in the A_1 phase.

The values of T_1^{-1} extracted from τ acquired via the MSE method and shown in Fig. 9 are plotted as a function of $(T-T_{C2})/T_{C2}$ in Fig. 14. The data from the MSE method are chosen because of the greater range of magnetic field than can be applied. Although there is some scatter, the experimentally determined relaxation rate shown in Fig. 14 can be

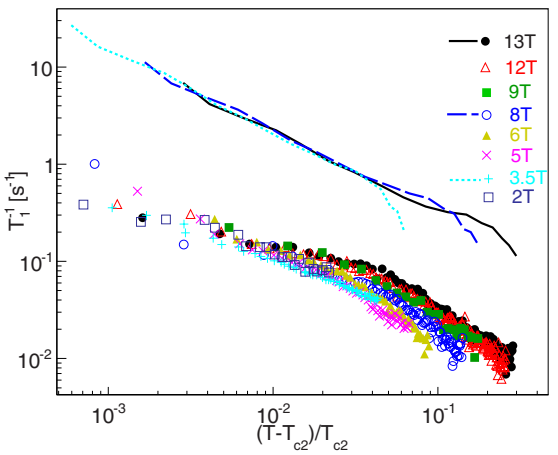

FIG. 14. (Color online) Values of T_1^{-1} vs reduced temperature $(T-T_{C2})/T_{C2}$ for the data shown in Fig. 9 and the same symbols used for each applied field. Note the change in the abscissa from the normalized reduced temperature r in Fig. 13. Theoretical relaxation rates (see text) are shown by lines at 3.5 (dotted), 8 (dashed), and 13 (solid) T.

simply represented by $T_1^{-1} \propto [(T-T_{C2})/T_{C2}]^{-\beta}$ with $\beta \sim 0.6$ in the restricted temperature range close to T_{C2} where $(T-T_{C2})/T_{C2} \lesssim 0.02$.

The argument for the minority spin condensate in the A_1 phase as the origin of the T_1^{-1} increase near T_{C2} is briefly as follows. MT (Ref. 14) showed that the small but finite minority spin condensate emerged when the dipolar interaction energy was included in the total free energy. The presence of both majority and minority pair condensates implied that a longitudinal magnetic resonance (with frequency $\Omega_\parallel$), which otherwise would be absent without the minority condensate, could occur in the A_1 phase.[14] The presence of a minority condensate then allows the Leggett-Takagi (LT) mechanism[27] to contribute in the spin-relaxation process, and consequently the spin-relaxation rate can dramatically increase.

According to the LT mechanism, the spin-density relaxation rate ($\Gamma_\parallel$) of a longitudinal magnetic resonance in the A phase is given by $\Gamma_\parallel = (1-\lambda)\tau_{qp}\Omega_\parallel^2/2\lambda(1+\zeta/4)$. Here, $\lambda = 1-Y_2(T)$, where Y_2 is the "second-order" Yosida function,[27] τ_{qp} the quasiparticle relaxation time[1] (to be assumed equal to that at T_{C1}), $(1+\zeta/4)^{-1}$ is the ratio of liquid magnetic susceptibility[1] to the ideal Fermi gas susceptibility and ζ is a Landau parameter. In the spirit of the quasistatic treatment of our experiment, we have hypothesized[28] that the measured T_1^{-1} be identified with $\Gamma_\parallel$.

MT computed the temperature dependence of $\Omega_\parallel(r_1)$ with $r_1 \equiv 1-r$ and found it to be independent of magnetic field up to 2 T (cf. Fig. 5 of Ref. 14). By computing $\lambda(T)$ for each applied field and assuming $\Omega_\parallel(r_1)$ is independent of field up to 13 T, the theoretical relaxation rate $\Gamma_\parallel$ is evaluated *without* adjusting any parameters and shown by the lines drawn on Fig. 14. The temperature dependence of the theoretical $\Gamma_\parallel$ agrees generally with the experimentally extracted values of T_1^{-1}. Insensitivity to applied field in the theory appears to be consistent with the experiment close to T_{C2} but not at higher temperatures. However, the overall magnitudes do not agree. If the minority energy gap $\Delta_{\downarrow\downarrow}$ were reduced by a factor 16, the theoretical prediction for $\Gamma_\parallel$ can be brought into agreement with the experimental data for T_1^{-1}. It is possible that the $\Omega_\parallel$ calculated by MT for the bulk A_1 phase may be different than that in our finite cell geometry contributing to the discrepancy.

The pressure dependence of T_1^{-1} extracted from τ at $r=0.5$ and 0.8 under an applied field of 8 T is shown in Fig. 15. The lines indicate the theoretical pressure dependence based on the presence of a minority spin condensate as follows. According to MT, $\Omega_\parallel^2$ in the A_1 phase is estimated as $\sim \gamma^2(g_D/\chi)\Delta_{\uparrow\uparrow}\Delta_{\downarrow\downarrow}$, where g_D is the dipolar energy[14] and the minority spin condensate energy gap $\Delta_{\downarrow\downarrow} \approx (g_D/\eta' H)\Delta_{\uparrow\uparrow}$. The term $\eta' H$ gives a measure of the transition temperature T_{C1} in magnetic field H.[14] It can then be shown $\Omega_\parallel^2 \sim (\gamma^2 g_D^2/\chi\beta_{24})(1-r/r_c)$, where $\beta_{24} = \beta'_{24}(21\zeta(3)/40\pi^2)(N(0)/k_B^2T_c^2)$, β'_{24} is a strong-coupling parameter,[29,30] $N(0)$ is the density of states, T_c is the transition temperature in zero field, and $r_c \equiv (T_{C1}-T_C)/T_C$. The pressure dependence of g_D/χ can be estimated from the measured temperature dependence of the longitudinal resonance frequency in the A phase as the temperature approaches T_c.[31] The theoretical pressure dependence of $\Gamma_\parallel$ divided by 16 is

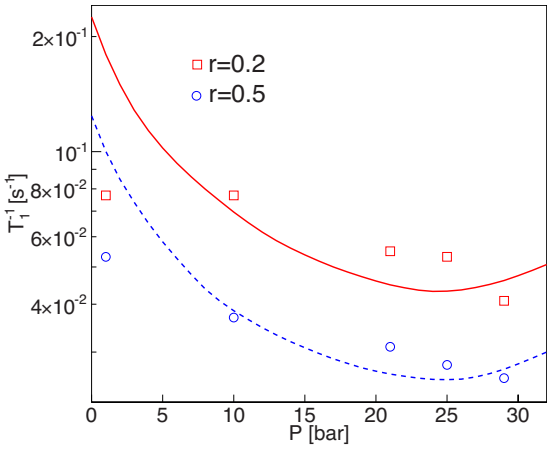

FIG. 15. (Color online) Measured pressure dependence of T_1^{-1} at 8 T and normalized reduced temperatures of 0.2 (red squares) and $r=0.5$ (blue circles). The scaled theoretical pressure dependence (see text) is shown by solid and dotted curves for $r=0.2$ and 0.5, respectively.

shown by the curves drawn on Fig. 15. The observed dependence of T_1^{-1} on pressure is thus roughly consistent with the theoretical expectation.

V. SUMMARY

We demonstrated that temperature gradients had been present in our previous MFE experiments[13] and that these gradients had influenced data in the ferromagnetic superfluid ^{3}He A_1 phase. The work presented here was motivated by the goal of eliminating these temperature gradients. The temperature gradients were successfully eliminated by replacing almost all of the epoxy that was in contact with superfluid ^{3}He in the previous apparatus by machinable ceramic (Macor). The important observations made previously[13] in which the spin-relaxation time tended to vanish as the A_1-A_2 phase transition temperature is approached was observed to persist when the temperature gradients were eliminated. The detection scheme was modified to permit observations of the MSE where mechanical spin pumping of the spin-polarized superfluid component of the A_1 phase was generated by electrostatically actuated membrane motion. The new measurements characterizing the MSE demonstrated that the same magnetic relaxation processes could be observed without imposing magnetic field gradients as required by the MFE experiments. The spin-relaxation rate (T_1^{-1}) was extracted as functions of temperature, pressure, and magnetic field. The temperature dependence of the extracted rate T_1^{-1} agrees well with that deduced by a formulation combining Leggett-Takagi spin dynamics with the existence of minority spin condensate as predicted by Monien and Tewordt. Our observations call for more theoretical studies of the minority spin condensate in the A_1 phase and of the exact relationship between minority spin condensate and the LT mechanism. Experimental improvements in temperature regulation and faster response in the capacitance detection system is desirable in the future for probing the possible divergence of T_1^{-1} near T_{C2}.

ACKNOWLEDGMENTS

We thank A. Awobode, H. Ebisawa, W. Halperin, A. Leggett, K. Nagai, and T. Takagi for discussions. This research was supported by JSPS Grant-in-Aid Scientific Research funds (Grants No. 19340091 and No. 22684019) and by the U.S. NSF (Grant No. DMR-0704120) and INT-NSF (Grant No. INT-0234032).

*Present address: Department of Material Science and Engineering, Tokyo Institute of Technology, Nagatsuta, Midori Yokohama 226-0026 Japan.

†Present address: Graduate School of Material Science, University of Hyogo, Kamigori Hyogo 678-1297 Japan.

[1] J. C. Wheatley, Rev. Mod. Phys. **47**, 415 (1975).
[2] A. J. Leggett, Rev. Mod. Phys. **47**, 331 (1975).
[3] V. Ambegaokar and N. D. Mermin, Phys. Rev. Lett. **30**, 81 (1973).
[4] M. Liu, Phys. Rev. Lett. **43**, 1740 (1979).
[5] L. R. Corruccini and D. D. Osheroff, Phys. Rev. Lett. **45**, 2029 (1980).
[6] M. Bastea, J. J. Coleman, P. G. N. DeVegvar, Y. Okuda, T. Sato, and H. Kojima, J. Low Temp. Phys. **137**, 539 (2004).
[7] R. Ruel and H. Kojima, Phys. Rev. Lett. **54**, 2238 (1985).
[8] A. Yamaguchi, S. Kobayashi, H. Ishimoto, and H. Kojima, Nature (London) **444**, 909 (2006).
[9] C.-R. Hu, Phys. Rev. Lett. **49**, 1493 (1982).
[10] A. V. Balatsky and B. L. Altshuler, Phys. Rev. Lett. **70**, 1678 (1993).
[11] H. Kojima and H. Ishimoto, J. Phys. Soc. Jpn. **77**, 111001 (2008).
[12] A. Yamaguchi, Y. Aoki, S. Murakawa, H. Ishimoto, and H. Kojima, Phys. Rev. B **80**, 052507 (2009).
[13] A. Yamaguchi, S. Kobayashi, H. Ishimoto, and H. Kojima, J. Low Temp. Phys. **148**, 513 (2007).
[14] H. Monien and L. Tewordt, J. Low Temp. Phys. **60**, 323 (1985).
[15] T. Dombre and R. Combescot, J. Phys. C **15**, 6925 (1982).
[16] R. Ruel and H. Kojima, Phys. Rev. B **28**, 6582 (1983).
[17] A. Yamaguchi, Y. Aoki, K. Suzuki, H. Ishimoto, and H. Kojima, J. Phys.: Conf. Ser. **150**, 032122 (2009).
[18] M. Grabinski, Phys. Rev. Lett. **63**, 814 (1989).
[19] F. A. Bais and A. M. J. Schakel, J. Phys.: Condens. Matter **2**, 5053 (1990).
[20] M. Schwark, F. Pobell, M. Kubota, and R. M. Mueller, J. Low Temp. Phys. **58**, 171 (1985).
[21] H. H. Jensen, H. Smith, P. Wolfle, K. Nagai, and T. M. Bisgaard, J. Low Temp. Phys. **41**, 473 (1980).
[22] A. J. Dahm, D. S. Betts, D. F. Brewer, J. Hutchins, S. J. Saunders, and W. S. Truscott, Phys. Rev. Lett. **45**, 1411 (1980).
[23] A. J. Leggett and M. Vuorio, J. Low Temp. Phys. **3**, 359 (1970).
[24] Y. Hu, G. J. Stecher, T. J. Gramila, and R. C. Richardson, Phys.

Rev. B **54**, R9639 (1996).
[25] L. P. Roobol, P. Remeijer, S. C. Steel, R. Jochemsen, V. S. Shumeiko, and G. Frossati, Phys. Rev. Lett. **79**, 685 (1997).
[26] A. Awobode and A. J. Leggett, APS March Meeting, BAPS, 2009.MAR.X16.9, http://meetings.aps.org/link/BAPS.2009.MAR.X16.9.
[27] A. J. Leggett and S. Takagi, Ann. Phys. **106**, 79 (1977).
[28] The longitudinal relaxation rate $\Gamma_{\parallel}^{-1}$ was derived (Ref. 27) for small changes in magnetic field, whose associated energy is small compared to the dipolar energy of order $\chi\Omega_{\parallel}^2/\gamma^2$. The changes in energy induced by the applied field gradient or by the pumped spin in our experiment is considerably greater than the dipolar energy. Nevertheless, the relaxation rate the $\Gamma_{\parallel}^{-1}$ appears to be nearly applicable to our experiment. The justification for this apllicability is not yet clear to us.
[29] H. Akimoto, T. Okuda, and H. Ishimoto, Phys. Rev. B **55**, 12635 (1997).
[30] Y. H. Tang, I. Hahn, H. M. Bozler, and C. M. Gould, Phys. Rev. Lett. **67**, 1775 (1991).
[31] P. Schiffer, M. T. O'Keefe, H. Fukuyama, and D. D. Osheroff, Phys. Rev. Lett. **69**, 3096 (1992).